SANDIA REPORT

SAND2010-6747
Unlimited Release
Printed September, 2010

Algorithm and Exploratory Study of the Hall MHD Rayleigh-Taylor Instability

Thomas A. Gardiner

Prepared by
Sandia National Laboratories
Albuquerque, New Mexico 87185 and Livermore, California 94550

Sandia National Laboratories is a multi-program laboratory managed and operated by Sandia Corporation, a wholly owned subsidiary of Lockheed Martin Corporation, for the U.S. Department of Energy's National Nuclear Security Administration under contract DE-AC04-94AL85000.

Sandia National Laboratories

Issued by Sandia National Laboratories, operated for the United States Department of Energy by Sandia Corporation.

Available to DOE and DOE contractors from
U.S. Department of Energy
Office of Scientific and Technical Information
P.O. Box 62
Oak Ridge, TN 37831

Telephone: (865) 576-8401
Facsimile: (865) 576-5728
E-Mail: reports@adonis.osti.gov
Online ordering: http://www.osti.gov/bridge

Available to the public from
U.S. Department of Commerce
National Technical Information Service
5285 Port Royal Rd
Springfield, VA 22161

Telephone: (800) 553-6847
Facsimile: (703) 605-6900
E-Mail: orders@ntis.fedworld.gov
Online ordering: http://www.ntis.gov/help/ordermethods.asp?loc=7-4-0#online

SAND2010-6747
Unlimited Release
Printed September, 2010

Algorithm and Exploratory Study of the Hall MHD Rayleigh-Taylor Instability

Thomas A. Gardiner

Abstract

This report is concerned with the influence of the Hall term on the nonlinear evolution of the Rayleigh-Taylor (RT) instability. This begins with a review of the magnetohydrodynamic (MHD) equations including the Hall term and the wave modes which are present in the system on time scales short enough that the plasma can be approximated as being stationary. In this limit one obtains what are known as the electron MHD (EMHD) equations which support two characteristic wave modes known as the whistler and Hall drift modes. Each of these modes is considered in some detail in order to draw attention to their key features. This analysis also serves to provide a background for testing the numerical algorithms used in this work. The numerical methods are briefly described and the EMHD solver is then tested for the evolution of whistler and Hall drift modes. These methods are then applied to study the nonlinear evolution of the MHD RT instability with and without the Hall term for two different configurations. The influence of the Hall term on the mixing and bubble growth rate are analyzed.

Contents

Figures

1 Introduction

When a light fluid supports a heavy fluid against a gravitational field the system is subject to the Rayleigh-Taylor (RT) instability. This same instability is present if a light fluid is used to accelerate a heavy fluid. In the classical description of the hydrodynamic instability the motion is the fluid is incompressible and the system is characterized by a single dimensionless quantity known as the Atwood number

$$A = \frac{\rho_h - \rho_l}{\rho_h + \rho_l} \tag{1}$$

where ρ_h and ρ_l are the densities in the heavy and light fluid respectively. The growth rate of this instability

$$\gamma = \sqrt{Agk} \tag{2}$$

where g is the gravitational acceleration and k is the magnitude of the wave vector.

When a uniform magnetic field is introduced into this picture aligned parallel to the interface it has a stabilizing influence. In this case, the growth rate becomes

$$\gamma^2 = Agk - \frac{(\mathbf{B}\cdot\mathbf{k})^2}{2\pi\mu_0(\rho_l + \rho_h)} \tag{3}$$

For wave vectors orthogonal to the magnetic field one recovers the hydrodynamic growth rate, while for wave vectors which are not orthogonal to the magnetic field we see that the magnetic tension acts to stabilize the perturbations driven by the gravitational field. From this relation for the growth rate we also see that there is a critical length scale below which perturbations are stabilized. For wave vectors parallel to the magnetic field this critical wavelength is given by

$$\lambda_c = \frac{B^2}{\mu_0(\rho_h - \rho_l)g} \tag{4}$$

While this linear behavior is well known, and very well reproduced by numeral simulation codes, the nonlinear, three-dimensional behavior of this system is particularly complex on length scales a few times longer than the critical wavelength [14].

When the Hall term is included into an MHD description of a plasma, it has been shown that there is a profound change to the traditional MHD RT instability [7, 8, 9]. At wavelengths large compared to the ion inertial length c/ω_{pi}, the instability recovers the ideal MHD behavior. For wavelengths small compared the the ion inertial length the instability takes on a new character. The unstable modes change from being incompressible to compressible fluctuations and their growth rate tends toward

$$\gamma \simeq \sqrt{gk/A} \tag{5}$$

which is larger than the traditional RT instability growth rate by a factor of $1/A$.

There are a variety of physical systems in which the RT instability is a key physical phenomenon. Z-pinch implosions are one such system where it is well known that the traditional

MHD RT instability is of key importance to obtaining stable compressions. In a z-pinch since the magnetic field is responsible for accelerating the heavy fluid, say a liner, a simple application of the planar stability criterion discussed above indicates that the critical wavelength, which determines whether the instability will be essentially two- or three-dimensional, is related to the ratio of the thickness to the radius of the liner. The large scale, gross morphological evolution of an imploding liner is quite reasonably well described by a resistive MHD model, though there may be periods of its implosion history for which the Hall term is important [10]. The Hall term is also expected to be important for an accurate description of the plasma ablated from the liner surface, the implosion of wire arrays, gas puffs, or the evolution near stagnation [13, 12].

This report is concerned with identifying the influence of the Hall term on the nonlinear evolution of the MHD RT instability. The report begins with a brief description of Hall MHD. This is followed by a description of the wave modes present in the electron MHD limit in order to clarify the manner in which the Hall term influences the magnetic field evolution. The numerical algorithm used in this paper for studying the Hall MHD RT instability is then outlined and results are presented for the evolution of the whistler and Hall drift modes. The following section presents results comparing ideal MHD and Hall MHD RT instability simulations. This report concludes with an outlook toward future research.

2 Hall MHD Equations and Wave Modes

In this study we will be concerned with the time-dependent evolution of a compressible, Hall MHD fluid governed by the following equations

$$\frac{\partial \rho}{\partial t} + \nabla \cdot (\rho \mathbf{v}) = 0 \tag{6}$$

$$\frac{\partial \rho \mathbf{v}}{\partial t} + \nabla \cdot \left(\rho \mathbf{v}\,\mathbf{v} - \frac{\mathbf{B}\,\mathbf{B}}{\mu_0} \right) + \nabla \left(P + \frac{B^2}{2\mu_0} \right) = 0 \tag{7}$$

$$\frac{\partial \mathbf{B}}{\partial t} + \nabla \times \left(\mathbf{B} \times \mathbf{v} + \frac{m_i}{Ze\rho} \mathbf{J} \times \mathbf{B} \right) = 0 \tag{8}$$

where ρ is the mass density, $\mathbf{v}$ is the center of mass plasma velocity, P is the pressure, $\mathbf{B}$ is the magnetic field, $\mathbf{J}$ is the current density, and Ze/m_i is the ion charge to mass ratio. The current density is given by Ampère's law neglecting the displacement current

$$\mathbf{J} = \frac{1}{\mu_0} \nabla \times \mathbf{B} \tag{9}$$

as is common in the MHD approximation. Finally, this system is typically closed by including a total energy equation and an equation of state relating the internal energy, mass density and pressure. In the problems presented here we will specialize to an isothermal equation of state where $P = a^2 \rho$ and a is the constant, isothermal sound speed.

This set of equations are distinguished from the traditional MHD equations by the addition of the last term in equation 8 which is the Hall electric field. Physically speaking, the Hall term accounts for the relative velocity of the electrons and ions. When the Hall term is included, the magnetic field is no longer tied to the center of mass reference frame, rather it is tied to the reference frame of the electrons. This seemingly small change can significantly alter the solutions relative to ideal MHD.

The isothermal MHD equations support 6 eigenmodes which come in pairs and are referred to as the fast, Alfvén and slow modes. When the Hall term is included, the eigenmodes are altered profound ways. While a complete analysis of the wave mode structure for Hall MHD is beyond the scope of the report, it is useful for both illustrative and testing purposes to consider the small time scale limit in which we can consider the plasma density, pressure and velocity to be fixed in time and the magnetic field evolves solely due to the Hall term. This limit is typically referred to as the electron MHD (EMHD) limit and the governing equation (for a stationary plasma) is

$$\frac{\partial \mathbf{B}}{\partial t} + \nabla \times \left(\frac{m_i}{Ze\rho} \mathbf{J} \times \mathbf{B} \right) = 0 \tag{10}$$

This equation supports two basic wave modes which are referred to as the whistler and the Hall drift mode and we consider each of these in turn.

2.1 Whistler Modes

Consider the propagation of a plane wave a uniform, stationary plasma with a background mean magnetic field. We choose a coordinate system with the x-axis aligned with the wave propagation direction. In this limit, the EMHD equations reduce to

$$B_x = \text{constant} \tag{11}$$

$$\frac{\partial B_y}{\partial t} - \left(\frac{m_i B_x}{\mu_0 Ze\rho}\right)\frac{\partial^2 B_z}{\partial x^2} = 0 \tag{12}$$

$$\frac{\partial B_z}{\partial t} + \left(\frac{m_i B_x}{\mu_0 Ze\rho}\right)\frac{\partial^2 B_y}{\partial x^2} = 0 \tag{13}$$

Defining $\psi = B_y - iB_z$ where $i = \sqrt{-1}$ this set of equations can be written as

$$\frac{\partial \psi}{\partial t} - i\left(\frac{m_i B_x}{\mu_0 Ze\rho}\right)\frac{\partial^2 \psi}{\partial x^2} = 0 \tag{14}$$

This is essentially the one-dimensional Schrödinger equation for a free particle. The eigenmodes are plane waves $\exp(ikx - i\omega t)$ with a dispersion relation

$$\omega = \left(\frac{m_i B_x}{\mu_0 Ze\rho}\right)k^2 \tag{15}$$

At this point there are a number of things worth noting about these wave modes. First, from the $\pi/2$ phase shift between B_y and B_z we see that these whistler modes are circularly polarized waves. Second, we see that whistler modes are dispersive with a phase velocity ω/k that increases linearly with k. That is, the shortest wavelength modes propagate with the highest phase velocity. Third, if we define an Alfvén velocity as

$$V_a = \frac{B_x}{\sqrt{\mu_0 \rho}} \tag{16}$$

then the whistler mode dispersion relation is (for $m_i \gg m_e$) approximately

$$\omega = k^2 \lambda_i V_a \tag{17}$$

where $\lambda_i = c/\omega_{pi}$ is the ion inertial length and

$$\omega_{pi} = \left(\frac{n_i (Ze)^2}{m_i \epsilon_0}\right)^{1/2} \tag{18}$$

Thus, we see that whistler modes will be important on length scales comparable or smaller than the ion inertial length.

2.2 Hall Drift Modes

To describe Hall drift modes we must consider an inhomogeneous plasma in at least two dimensions. Let the y-direction be an ignorable coordinate, i.e.

$$\frac{\partial}{\partial y} = 0 \tag{19}$$

in an operator sense. Furthermore, we will restrict the magnetic field such that $\mathbf{B} = B_y\hat{\mathbf{j}}$ which allows us to simplify the Hall electric field as

$$\mathbf{E}_H = \left(\frac{m_i}{\mu_0 Ze\rho}\right)\left(-\nabla\frac{B^2}{2}\right) \tag{20}$$

The EMHD equations thus become

$$\frac{\partial \mathbf{B}}{\partial t} + \nabla \times \left(\frac{m_i}{\mu_0 Ze\rho}\left(-\nabla\frac{B^2}{2}\right)\right) = 0 \tag{21}$$

which using the fact that $\nabla \times \nabla = 0$ can be rewritten as

$$\frac{\partial \mathbf{B}}{\partial t} + \nabla \times \left(\left(\nabla\frac{m_i}{\mu_0 Ze\rho}\right)\frac{B^2}{2}\right) = 0 \tag{22}$$

At this point it is worth noting that for the configuration considered here, the EMHD equations have reduced to a nonlinear hyperbolic system. In fact, when

$$\nabla\frac{m_i}{Z\rho} = constant \tag{23}$$

this is essentially Burgers' equation. Hence, these Hall drift wave modes are nonlinear waves and can lead to wave steepening, shocks, rarefactions, etc. It is important to note that this demonstrates that weak solutions to the EMHD equations which contain Hall drift modes are dissipative, despite the fact that $\mathbf{J} \cdot \mathbf{E}_H = 0$.

If we define $n = Z\rho/m_i$, equation 22 can be written in semi-linear form as

$$\frac{\partial B_y}{\partial t} - \frac{B_y}{\mu_0 n^2 e}\left(\frac{\partial n}{\partial x}\right)\frac{\partial B_y}{\partial z} \tag{24}$$

$$+ \frac{B_y}{\mu_0 n^2 e}\left(\frac{\partial n}{\partial z}\right)\frac{\partial B_y}{\partial x} = 0 \tag{25}$$

Thus, we find that the Hall drift mode velocity in the z-direction is given by

$$V_z^{Hd} = -\frac{m_i B_y}{\mu_0 Ze\rho L_x} \tag{26}$$

where

$$L_x = \left(\frac{\partial \ln n}{\partial x}\right)^{-1} \tag{27}$$

is the characteristic length scale in the x-direction. Similarly, the Hall drift mode velocity in the x-direction is given by

$$V_x^{Hd} = \frac{m_i B_y}{\mu_0 Ze\rho L_z} \tag{28}$$

with a similar definition for the characteristic length scale in the z-direction. Normalizing the Hall drift mode speed to a characteristic Alfvén speed

$$V_a = \frac{B_y}{\sqrt{\mu_0 \rho}} \tag{29}$$

we find that the Hall drift mode wave speed can be written as

$$V^{Hd} = V_a \left(\frac{\lambda_i}{L} \right) \tag{30}$$

where λ_i is the ion inertial length and

$$L = \left(\frac{\partial \ln n}{\partial x_\perp} \right)^{-1} \tag{31}$$

is a characteristic length scale in a direction orthogonal to both B and the wave propagation direction. Again, we find that the Hall electric field will be important for length-scales comparable to the ion inertial length scale.

3 Numerical Method and Test Problems

In this work we will be using an operator splitting approach for solving the Hall MHD equations. The splitting will use two operators, an unsplit ideal MHD evolution operator [5, 6] and an EMHD evolution operator developed as part of this work. The ideal MHD solver uses a higher order Godunov method based on the Corner Transport Upwind (CTU) method of Colella [3] which evolves the usual hydrodynamic variables as cell volume average quantities and the method of Constrained Transport (CT) [4] which evolves the interface normal components of the magnetic field as cell face average quantities. The CT algorithm guarantees the divergence free constraint on the magnetic field to roundoff error.

The EMHD algorithm developed here is inspired by the work of [11] which demonstrated that it is possible to construct stable, explicit methods for the EMHD equations despite the apparently singular nature for the whistler mode dispersion relation. One of the key features identified by O'Sullivan and Downes [11] is that due to the skew-symmetric nature of the EMHD equations, the numerical algorithm stability properties are greatly improved by staggering the update to the magnetic field components. In fact, in one-dimension evolving the the two transverse components of the magnetic field using the Verlet method is a stable, symplectic integration algorithm. This can also be understood from the point of view that in one-dimension only the whistler modes are accessible and as noted in the section on whistler modes in this limit the EMHD equations can be rewritten in a form equivalent to Schrödinger's equation for a free particle. Hence, the symplectic methods for Schrödinger's equation [2] are also applicable in this limit. In more than one dimension, however, evolving the magnetic field components independently breaks the divergence free character of the magnetic field, hence breaking the CT method.

Interestingly enough, a staggered update method can be employed if one simply evolves a different set of equations. Consider the time integral of Faraday's equation from time t^n to time t

$$\mathbf{B} - \mathbf{B}^n + \nabla \times \int_{t^n}^{t} \mathbf{E}(t')\,\mathrm{d}t' = 0 \tag{32}$$

and let's define a new variable

$$\mathbf{K} = \int_{t^n}^{t} \mathbf{E}(t')\,\mathrm{d}t' \tag{33}$$

as a time integral of the electric field. Then the integral form of Faraday's law is given by the temporally algebraic relation

$$\mathbf{B} - \mathbf{B}^n + \nabla \times \mathbf{K} = 0\ . \tag{34}$$

Meanwhile, writing Ohm's law for the Hall electric field in terms of $\mathbf{K}$ we have a differential relation

$$\frac{\partial \mathbf{K}}{\partial t} = \frac{m_i}{Ze\rho}\mathbf{J} \times \mathbf{B} \tag{35}$$

If we substitute Ampére's law for the current density and the time-integrated form of Faraday's law for the magnetic field we obtain a closed system of equations which for $\mathbf{K}$ which

depends on the magnetic field at time t^n but does not contain any geometrical constraints. The result is the EMHD equations written in terms of the time-integrated electric field. Hence, a staggered update of the components of $\mathbf{K}$ can be employed within the CT framework.

3.1 Whistler Mode Test

In this section we test the solution behavior for the Hall whistler modes in a two-dimensional domain. We choose a uniform, stationary plasma background and simulate the whistler mode propagation in the (x, z)-plane with periodic boundary conditions. The computational domain extends from $0 \leq x \leq \sqrt{5}$ and $0 \leq z \leq \sqrt{5}/2$ and is resolved on a $2N \times N$ grid. The whistler mode propagates at an angle $\theta = \tan^{-1}(2) \approx 63.4^\circ$ with respect to the x-axis and has a wavelength $\lambda = 1$. The magnetic field components are most easily described in a rotated coordinate system (x_1, x_2, x_3) where

$$x_1 = x\cos\theta + z\sin\theta \tag{36}$$
$$x_2 = y \tag{37}$$
$$x_3 = -x\sin\theta + z\cos\theta \tag{38}$$

The magnetic field components

$$B_1 = 1 \tag{39}$$
$$B_2 = 0.1\cos(2\pi x_1) \tag{40}$$
$$B_3 = 0.1\sin(2\pi x_1) \tag{41}$$

Finally, we choose a set of units in which $\mu_0 = 4\pi$, $Ze/m_i = 0.1$, $\rho = 1$. With these choices the whistler mode phase velocity equals 5 and the orbital period equals $1/5$. We evolve this whistler mode on a grid with $N = 64$ for 100 orbital periods.

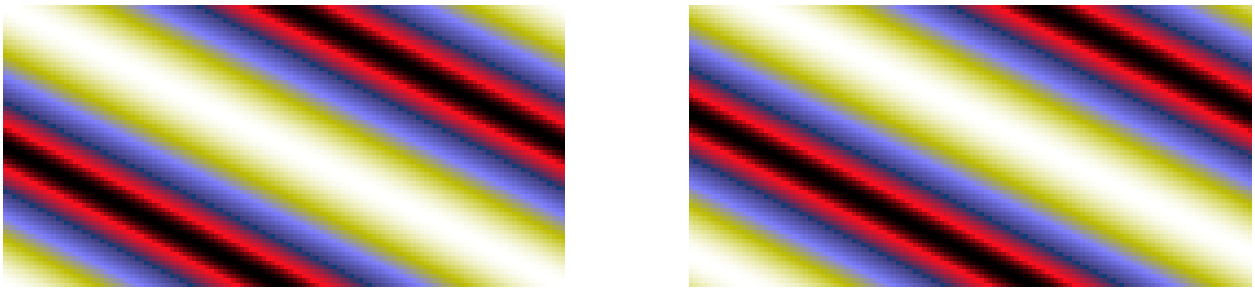

Figure 1. Image of B_y at time = 0 (left) and time = 100 orbital periods (right) for the oblique propagation of a whistler mode. The horizontal axis is the x-axis and the vertical axis is the z-axis.

In figure 1 we present images of B_y at time equal to zero and 100 orbital periods. From the images one can see that the wave is propagating along a direction oblique to the mesh and there is a slight phase shift from the initial to final solution. In figure 2 we present a line plot of B_y versus the propagation direction x_1 including every grid cell in the simulation. The lack of scatter in the plot demonstrates that the wave retains planar symmetry throughout the simulation. The amplitude of the wave shows no dissipation, i.e. there is no amplitude error in propagating this wave and the energy is conserved. Instead there is a phase error which causes the wave to propagate at a slightly slower speed than the analytic solution.

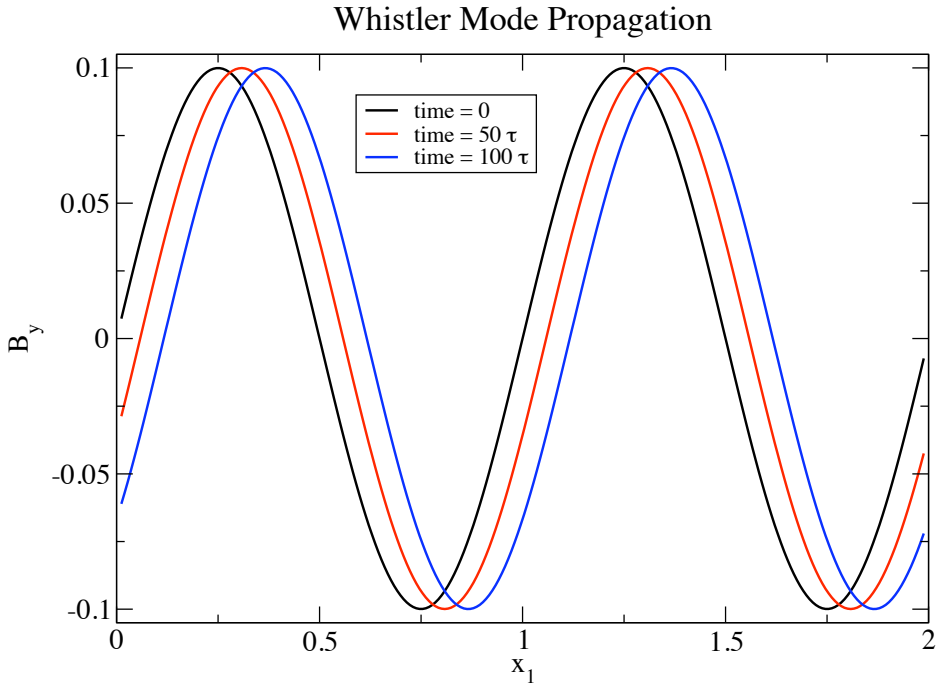

Figure 2. Plot of B_y along the wave propagation x_1 including *all* grid points at times $(0, 50, 100)$ orbital periods. The wave mode propagates without amplitude error, but some phase error.

3.2 Hall Drift Mode Test

We test the solution behavior for Hall drift modes by performing two-dimensional calculations in the (x, z)-plane with periodic boundary conditions. We choose a constant value for the ion charge to mass ratio and initialize the mass density

$$\rho = \rho_0 \left(1 + \delta \cos \left(\frac{2\pi z}{L_z} \right) \right) \tag{42}$$

and out-of plane magnetic field component

$$B_y = B_{y,0}\left(1 + \delta\cos\left(\frac{2\pi x}{L_x}\right)\right) \tag{43}$$

where the computational domain covers $-L_x/2 \le x \le L_x/2$ and $-L_z/2 \le z \le L_z/2$. From our previous analysis of the Hall drift mode, we expect the EMHD equations to evolve B_y according to

$$\frac{\partial B_y}{\partial t} + \frac{m_i B_y}{\mu_0 Z e \rho^2}\left(\frac{\partial \rho}{\partial z}\right)\frac{\partial B_y}{\partial x} = 0 \tag{44}$$

Along any given line $z =$ const. the magnetic field propagates in the x-direction according to Burgers' equation

$$\frac{\partial v}{\partial t} + v\frac{\partial v}{\partial x} = 0 \tag{45}$$

where the velocity v is the Hall drift wave velocity in the x-direction

$$v = -\frac{m_i B_y}{\mu_0 Z e \rho^2}\left(\frac{2\pi}{L_z}\right)\rho_0\delta\sin\left(\frac{2\pi z}{L_z}\right) \tag{46}$$

For our test problem we choose a set of units in which $\mu_0 = 4\pi$, $Ze/m_i = 0.1$, $\rho_0 = 1$, $B_{y,0} = 1$, $L_x = L_z = 1$ and $\delta = 0.1$. Then along the lines $z = \pm 1/4$ the Hall drift wave speed equals $\mp 1/2$ for $B_y = B_{y,0}$. In figure 3 we present a sequence of images of B_y at unit period intervals, times $(0, 2, 4, 6)$. From these images one can see that the Hall drift wave speed varies approximately sinusoidally in the z-direction. It is also apparent from the images that the Hall drift waves evolve into a weak solution. In figure 4 this is presented in a more quantitative manner by plotting B_y as a function of x for $z = -1/4$ for the same sequence of times. This demonstrates the evolution of a sine wave steepening into a weak solution (shock) characteristic of Burgers' equation. The flattening of the peaks of the wave are a result of the use of a min-mod limiter and the use of a less dissipative limiter could improve this. Nevertheless, the code accurately captures the development of the magnetic shock wave without oscillations. Also, the alignment of the wave at intervals equal to the wave period demonstrates accurate wave speed resolution.

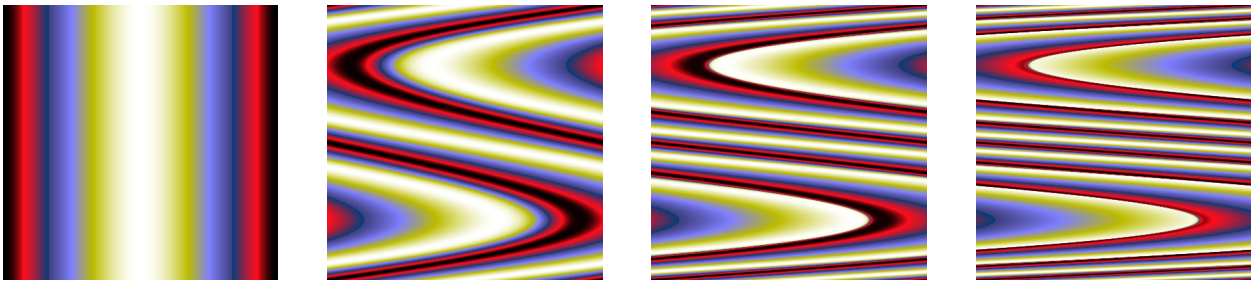

Figure 3. Sequence of images of B_y at times $(0, 2, 4, 6)$ from left to right. The horizontal axis is the x-axis and the vertical axis is the z-axis.

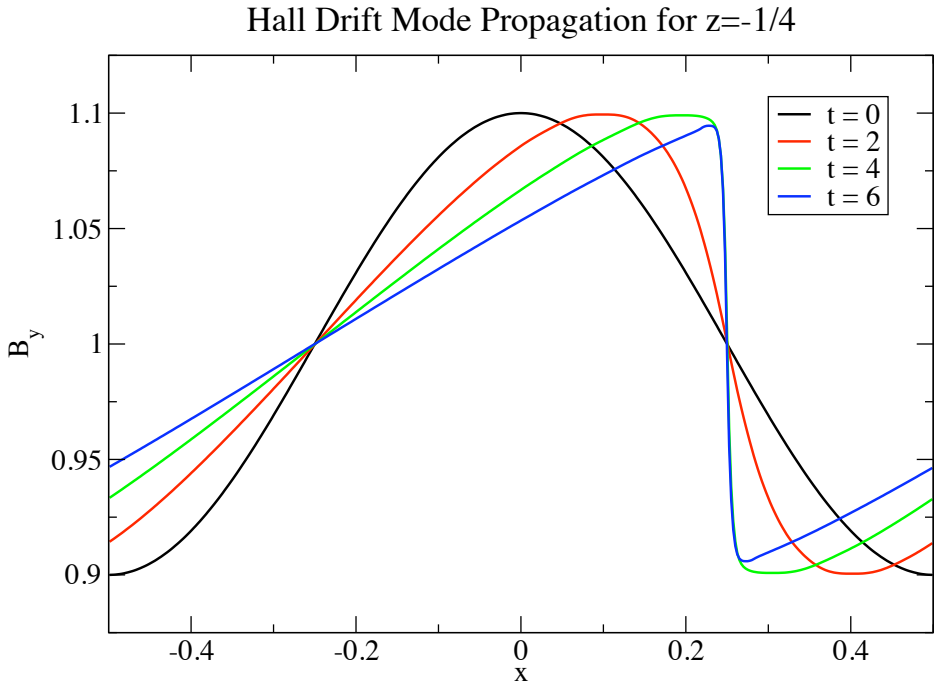

Figure 4. Plot of B_y along the line $z = -1/4$ at times $(0, 2, 4, 6)$ demonstrating the steepening of a sinusoidal wave to a shock.

4 Rayleigh-Taylor Instability Simulations

In this section we present results from simulating the Hall MHD Rayleigh-Taylor instability in two dimensions reproducing the calculations in [9]. To seed the instability the velocity is perturbed with uniformly random numbers with a maximum amplitude of approximately 2×10^{-5} of the isothermal sound speed. Ideal MHD simulations with identical initial conditions are also run. These serve as a reference from which we can understand the influence of the Hall term on the evolution of the instability.

4.1 Case 1

The first set of simulations is initialized with the following set of parameters; the Atwood number A=0.538, the grid dimensions $L_x = 148c/\omega_{pi}$ and $L_z = 74c/\omega_{pi}$, the ion plasma $\beta_i = 0.167$, and the normalized gravitational field strength $\hat{g} = 0.0115$ where the gravitational acceleration $g = \hat{g}\Omega_i V_a$, Ω_i is the ion cyclotron frequency, and V_a is the Alfvén speed with the density and magnetic field strength normalized to their values on the heavy side of the fluid interface. We use a mesh resolution of $(N_x, N_z) = (800, 400)$ so that the grid cell sizes $\delta x = \delta z$ and $c/\omega_{pi} = 5.4\delta x$. Note that these initial conditions contain a density discontinuity at the interface between the heavy and light fluids which will result in a Hall drift wave which propagates parallel to the interface. In the neighborhood of an interface, the density gradient (for the Hall MHD evolution) is approximated as a one-sided density gradient. Hence,

$$\left(\frac{\partial \ln \rho}{\partial z}\right) \approx \frac{2A}{\delta z} \tag{47}$$

and the Hall drift mode velocity in the x-direction is given by

$$V_x^{Hd} = V_a \left(\frac{2A\lambda_i}{\delta z}\right) \approx 5.8 V_a \tag{48}$$

at the interface between the heavy and light fluids. As a result magnetic field fluctuations at the interface will be rapidly transported along the interface between the heavy and light fluids.

In figure 5 the density for the ideal MHD and Hall MHD simulations are presented at three different times. The initial frame for the ideal MHD simulation is at time $\approx 130/\Omega_i$ while the initial frame for the Hall MHD simulation is at time $\approx 75/\Omega_i$ where the ion cyclotron frequency is evaluated in the initial state on the heavy fluid side of the interface. The time of the initial ideal MHD frame was chosen so as to make the amplitude of the interface perturbation comparable to the Hall MHD case. The time between frames is $\approx 100/\Omega_i$. The most apparent differences between the ideal and Hall MHD simulations has to do with the characteristic scale of the RT fingers. In the initial frame the RT fingers are approximately two times smaller in the ideal MHD case. Also, the width of the transition layer between the low and high density regions in the Hall MHD case is approximately two times larger

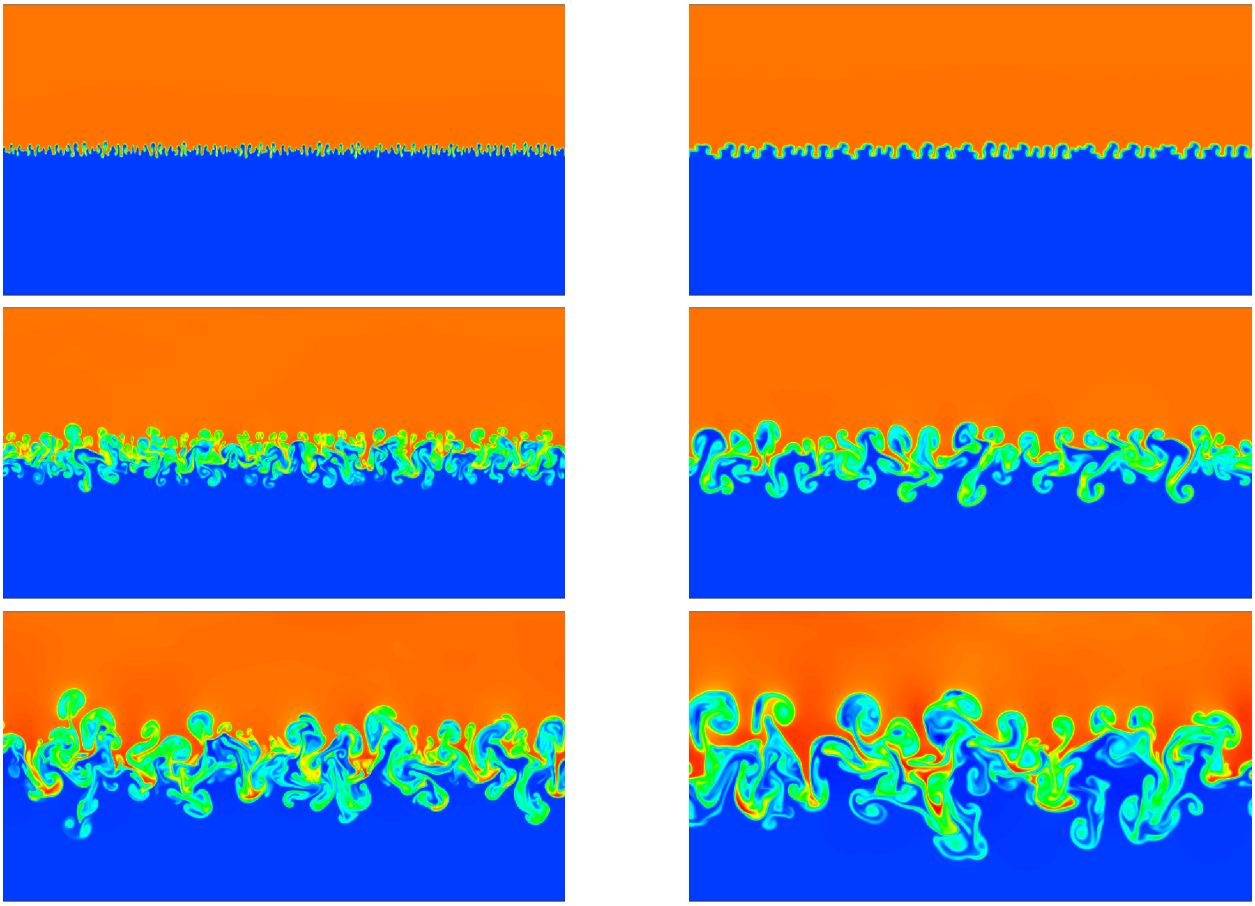

Figure 5. Plot of the mass density as a function of time for the ideal (left column) and Hall (right column) MHD RT instability. The initial frame is at time $130/\Omega_i$ and $75/\Omega_i$ for the ideal and Hall MHD simulation respectively. The time interval between images is $100/\Omega_i$.

than in the ideal MHD case. These characteristic differences carry forward in time as well with smaller scale features evident in the ideal MHD simulation results.

Two additional important characteristics of RT instability evolution are the rate at which initially heavy and light fluids are mixed and the growth rate of the bubbles. These can be quantified by tracking the heavy and light fluids independently during the course of the simulation. Numerically this is accomplished by simultaneously solving an additional set of mass conservation laws

$$\frac{\partial \rho f}{\partial t} + \nabla \cdot (\rho f \mathbf{v}) = 0 \tag{49}$$

where ρ is the mass density and $f = (f_l, f_h)$ for the light and heavy fluid fractions. Formally,

when also solving the continuity equation this is equivalent to solving the advection equations

$$\frac{\partial f}{\partial t} + \mathbf{v} \cdot \nabla f = 0 \tag{50}$$

though the former have certain numerical advantages. To quantify the mixing of the initially heavy and light fluids we define a horizontally averaged mixing parameter

$$\langle \Theta \rangle = \frac{1}{L_x} \int 4 f_l f_h \, \mathrm{d}x \tag{51}$$

which is defined such that $0 \leq \langle \Theta \rangle \leq 1$. One option is to plot this mixing parameter as a function of z at various times comparing the ideal and Hall MHD simulations. With this approach, however it is unclear if we should be comparing curves at the same time, or shifted times as was done for the images in figure 5. An alternative makes use of self-similarity arguments.

From self-similarity arguments, the height of the bubbles h above the initial interface is expected to scale as

$$h = \alpha A g t^2 \tag{52}$$

where α is a dimensionless number characterizing how the bubble evolution scales relative to free-fall. Formally it is not obvious that this should apply to the Hall MHD RT simulations except possibly in the limit of small ion inertial length $\lambda_i/h \ll 1$. Nevertheless, this scaling can be tested using the simulations themselves. We can exploit this self-similarity property by defining a dimensionless vertical coordinate $\hat{z} = z/(Agt^2)$. Self-similarity arguments imply that at late time, plots of $\langle \Theta \rangle$ versus $\hat{z}$ will be independent of time. In figure 6 the mixing parameter $\langle \Theta \rangle$ is plotted as a function of $\hat{z}$ at a number of different times spanning the interval of $100/\Omega_i$ near the end of the simulations. The plots demonstrate that temporal evolution of the mixing parameter is nearly self-similar at late time. The mixing of the heavy and light fluids near the origin is larger for ideal MHD compared to Hall MHD, which is likely due to the tendency toward developing smaller scale structures. On the other hand, the full width half maximum in the Hall MHD case is approximately 1.8 times larger than in the ideal MHD case. This can be understood as indicating that α is larger for Hall MHD than ideal MHD. This is consistent with plots of $< f_l >$ versus $\hat{z}$ which indicate that α for Hall MHD is approximately 1.7 times larger than α for ideal MHD.

4.2 Case 2

The second set of simulations is initialized with the following set of parameters; the Atwood number A=0.17, the grid dimensions $L_x = 18.8c/\omega_{pi}$ and $L_z = 9.4c/\omega_{pi}$, the ion plasma $\beta_i = 0.071$, and the normalized gravitational field strength $\hat{g} = 0.09$ where the gravitational acceleration $g = \hat{g}\Omega_i V_a$, Ω_i is the ion cyclotron frequency, and V_a is the Alfvén speed with the density and magnetic field strength normalized to their values on the heavy side of the fluid interface. These initial conditions differ from those used in [9] in the sense that the simulation domain in their study measured $12c/\omega_{pi}$ in the direction transverse to the gravitational field.

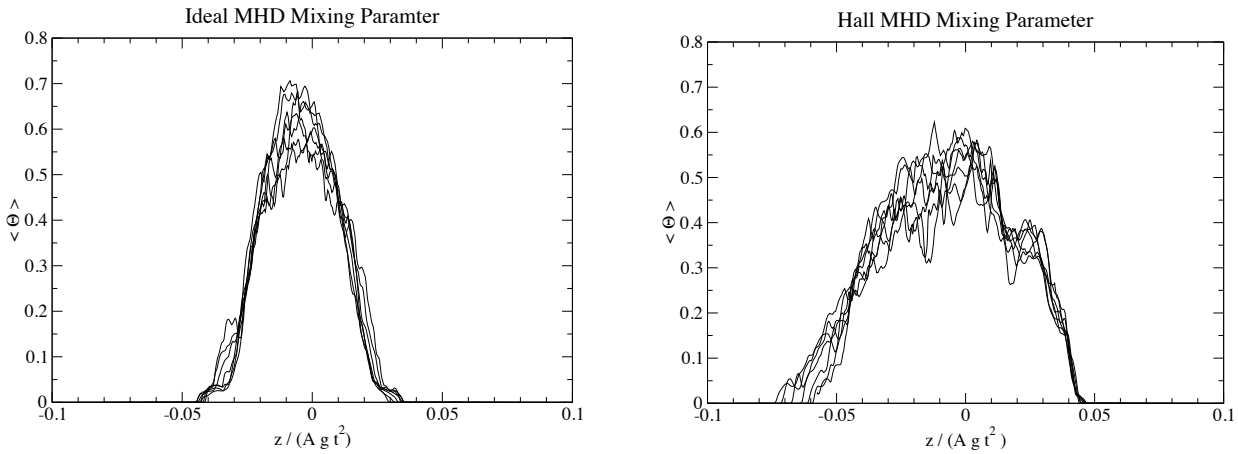

Figure 6. Plot shows the mixing parameter $\langle\Theta\rangle$ versus normalized $\hat{z}$ coordinate for ideal (left) and Hall (right) MHD RT instability. The curves span a time interval of $100/\Omega_i$ near the end of the simulation.

We use a mesh resolution of $(N_x, N_z) = (800, 400)$ so that the grid cell sizes $\delta x = \delta z$ and $c/\omega_{pi} = 42.6\delta x$. As with the first set of simulations, the initial density discontinuity implies the presence of a Hall drift wave with a velocity in the x-direction

$$V_x^{Hd} = V_a \left(\frac{2A\lambda_i}{\delta z} \right) \approx 14.5 V_a \tag{53}$$

at the interface between the heavy and light fluids.

In figure 7 the density at three different times is presented for both the ideal and Hall MHD RT simulations. As with the previous case, the times are chosen to characterize representative amplitudes of the instability. Again we find that the ideal MHD RT instability develops high-k bubbles and spikes which evolve through vortical motions. In this case, however, at late times the classical RT instability leads to compressible fluctuations as the sonic Mach number approaches 1 throughout the mixing region. In the Hall MHD RT simulations we find that only long wavelength fluctuations appear to grow at early time. As time progresses, the density in the RT instability appears reminiscent of a Kelvin-Helmholtz instability with a characteristic length scale $\sim 2c/\omega_{pi}$. At late times we also find a significant amount of compression though only long wavelength modes persist.

As with the previous case, we would like to measure the impact of the Hall term on the mixing and bubble growth rate. Unfortunately, plots of the horizontally averaged mixing parameter at late times indicate that the Hall MHD simulation never reaches a self-similar state. This is reasonable given the fact that the bubble height never becomes significantly larger than the ion inertial length. Instead, it is informative to simply plot the mixing parameter $\Theta = 4 f_l f_h$. This is shown for the ideal and Hall MHD simulations at late time in figure 8. From this figure it is clear that in the ideal MHD simulation there is a significant

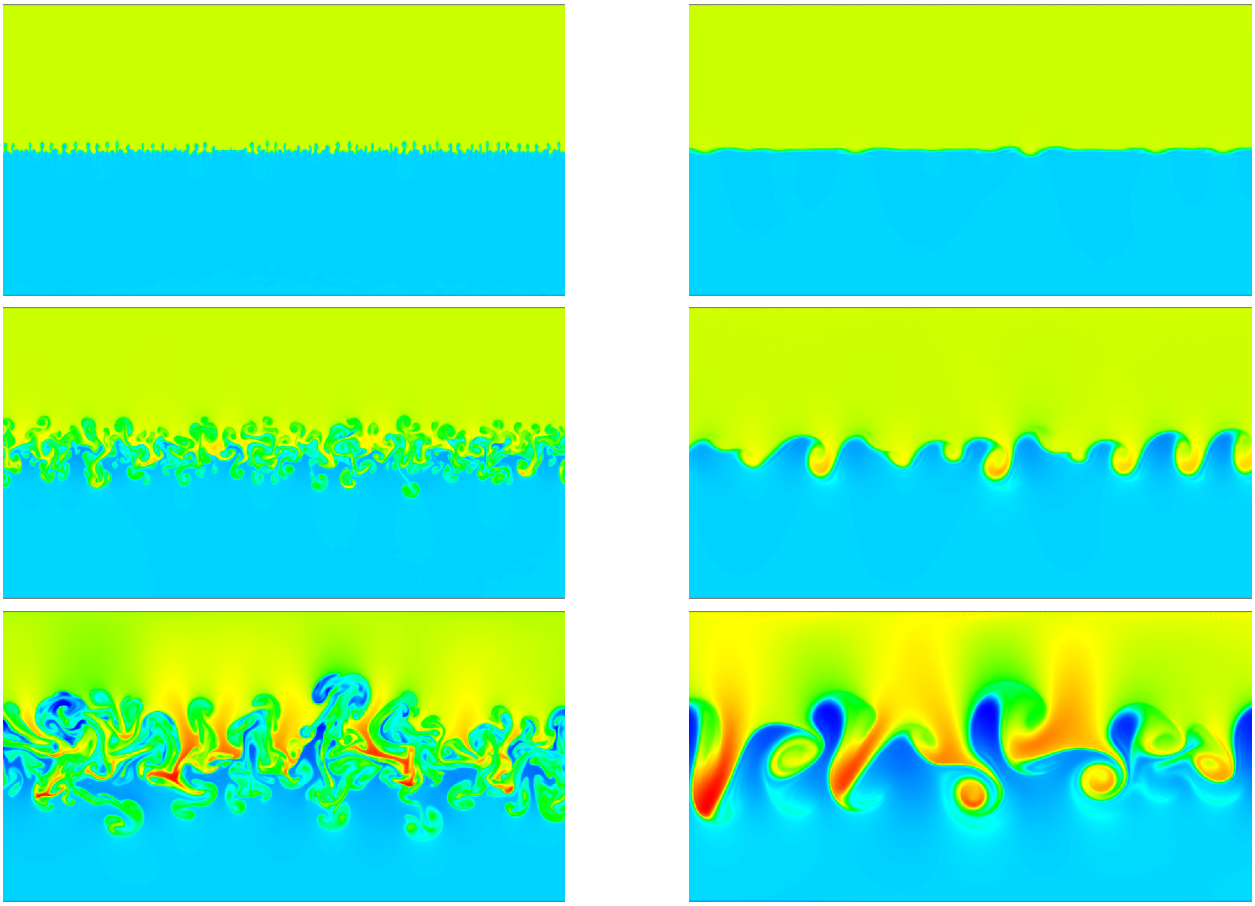

Figure 7. Plot of the mass density as a function of time for the ideal (left column) and Hall (right column) MHD RT instability. The ideal MHD images are at times $(70, 112, 155)/\Omega_i$ and the Hall MHD images are at times $(52, 73, 95)/\Omega_i$. A uniform color table is used for all images.

amount of mixing on small scales, while in the Hall MHD simulation the mixing only occurs at the boundary between the fluids and has a very regular pattern. Moreover, through a careful comparison of the density in figure 7 and the mixing parameter in figure 8 one finds that the boundary between the initially heavy and light fluids does not match the boundary between the low and high mass density regions in figure 7. This can be more clearly demonstrated by plotting the mass density $(\rho f_h, \rho f_l)$ for the initially heavy and light fluids respectively at late time. This is presented in figure 9 which interestingly enough shows that the highest mass density regions result from the compression of the initially light fluid into a smaller volume. Note also that it is a direct consequence of the Hall term since in ideal MHD the ratio B_y/ρ is a Lagrangian invariant for this two-dimensional configuration.

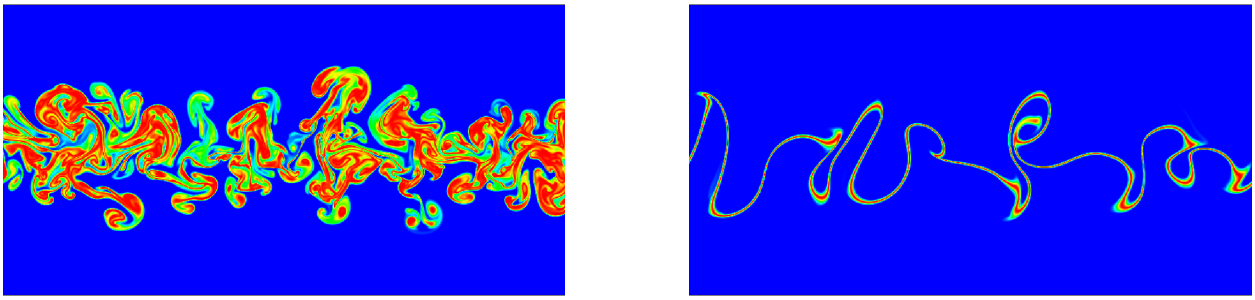

Figure 8. Plot of the mixing parameter $\Theta = 4 f_l f_h$ for the ideal (left) and Hall (right) MHD RT instability. The ideal and Hall MHD images are at time $155/\Omega_i$ and $95/\Omega_i$ respectively. The color scale varies from blue ($\Theta = 0$) with no mixing to red ($\Theta = 1$) with complete mixing.

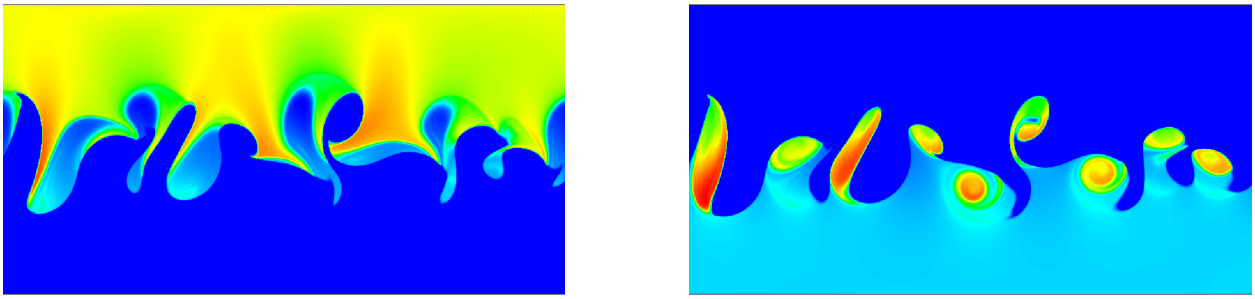

Figure 9. Plot of the mass density ρf_h in the initially heavy fluid (left) and the mass density ρf_l in the initially light fluid (right) in the Hall MHD RT simulation at time $95/\Omega_i$.

5 Summary and Discussion

In this report we have studied the evolution of the Hall MHD Rayleigh-Taylor instability in two dimensions and compared the results against ideal MHD RT simulations with identical initial conditions. This work began with a description of the Hall MHD equations and the wave modes which are present in the electron MHD limit. This analysis presented the two basic wave modes present in EMHD, the whistler and Hall drift mode. Each of these modes was shown to have a phase velocity given by the Alfvén speed times the ratio of the ion inertial length to a characteristic length scale indicating that Hall physics is important on length scales comparable to the ion inertial length. We further demonstrated that whistler modes are non-dissipative while Hall drift modes can be genuinely nonlinear resulting in the formation of rarefaction waves, self-steepening and magnetic shocks. Indeed, despite the fact that $\mathbf{J} \cdot \mathbf{E}_H = 0$, the Hall drift mode is dissipative for weak solutions. Making use of this analysis we tested the numerical algorithms used in this study on the propagation of whistler and Hall drift modes showing that both wave modes are well behaved. This work laid the foundation for having confidence in the numerical results presented in the remainder of the report on the nonlinear evolution of the Hall MHD RT instability.

In section §4 we presented results for the nonlinear evolution of the ideal and Hall MHD RT instability for two cases. These two cases have been presented previously in the literature [9]. In general terms we have found that the Hall term increases α and decreases mixing by suppressing the formation of small scale fluctuations. This is reasonably consistent with the linear theory, but a discrepancy remains with respect to the results presented in [9]. There it was noted that in case 2 with sufficiently high resolution the Hall term lead to the formation of a high wavenumber mode whose growth rate was consistent with linear theory. In contrast we have not observed the formation of this short wavelength mode even though we have run simulations (not presented here) with a mesh resolution equal to the highest resolution run used in [9]. The resolution of this discrepancy is left to future investigation.

The Hall MHD RT simulations in case 2 also demonstrated a surprising new result regarding the compressible nature of the instability. At early times both in this work and in [9] it was noted that the instability evolved in a way that was reminiscent of the Kelvin-Helmholtz (KH) instability. This is due to the appearance of what look like vortical patterns twisting up the high and low density regions. From this work we learned, however, that the similarity with the KH instability was in appearance alone. The high and low mass density regions at late time do not coincide with the initially high and low mass density regions at early time. In fact, the highest density regions were initially low mass density material which had been compressed. This phenomenon highlights the fact that in Hall MHD the magnetic field is stationary in the reference frame of the electron fluid, not the center of mass frame as is the case for ideal MHD.

A very interesting question for future research pertains to the fully three-dimensional character of the Hall MHD RT instability on length scales a few times larger than the critical wavelength where magnetic tension stabilizes the instability. As in the case of the ideal MHD RT instability, on these length scales the asymmetry in the evolution of the instability is

quite pronounced leading the the formation of arched magnetic flux ropes which rise or fall depending on their mass density. In the presence of the Hall term these flux ropes should be expected to interact as the magnetic field drifts with respect to the fluid. The exact nature of the interaction between these flux ropes in the three-dimensional case is unclear, but if they form current sheets they can be readily expected to result in fast magnetic reconnection [1]. In a low to moderate β plasma this dissipation should result in a significant perturbation to the dynamics. These results could hold significant implications for understanding the dynamics of the accretion disks, supernovae and z-pinch implosions.

References

[1] J. Birn, J. F. Drake, M. A. Shay, B. N. Rogers, R. E. Denton, M. Hesse, M. Kuznetsova, Z. W. Ma, A. Bhattacharjee, A. Otto, and P. L. Pritchett. Geospace environmental modeling magnetic reconnection challenge. *Journal of Geophysical Research*, 106(A3):3715 – 3719, 2001.

[2] S. Blanes, F. Casas, and A. Murua. Symplectic splitting operator methods for the time-dependent Schrödinger equation. *Journal of Chemical Physics*, 124(23):234105 – 234114, 2006.

[3] P. Colella. Multidimensional upwind methods for hyperbolic conservation laws. *Journal of Computational Physics*, 87(1):171 – 200, 1990.

[4] C. R. Evans and J. F. Hawley. Simulation of magnetohydrodynamic flows - A constrained transport method. *The Astrophysical Journal*, 332:659 – 677, September 1988.

[5] T. A. Gardiner and J. M. Stone. An unsplit Godunov method for ideal mhd via constrained transport. *Journal of Computational Physics*, 205(2):509 – 539, 2005.

[6] T. A. Gardiner and J. M. Stone. An unsplit Godunov method for ideal mhd via constrained transport in three dimensions. *Journal of Computational Physics*, 227(8):4123 – 4141, 2008.

[7] J. D. Huba. Hall magnetohydrodynamics in space and laboratory plasmas. *Physics of Plasmas*, 2(6):2504 – 2513, 1995.

[8] J. D. Huba, J. G. Lyon, and A. B. Hassam. Theory and simulation of the Rayleigh-Taylor instability in the limit of large Larmore radius. *Physical Review Letters*, 59(26):2971 – 2974, 1987.

[9] J. D. Huba and D. Winske. Rayleigh–Taylor instability: Comparison of hybrid and nonideal magnetohydrodynamic simulations. *Physics of Plasmas*, 5(6):2305 – 2316, 1998.

[10] B.V. Oliver and T.A. Mehlhorn. Nonideal MHD plasma regimes in the study of dynamic z pinches. *Plasma Science, IEEE Transactions on*, 30(2):517 – 523, apr. 2002.

[11] S. O'Sullivan and T. P. Downes. A three-dimensional numerical method for modelling weakly ionized plasmas. *Monthly Notices of the Royal Astronomical Society*, 376(4):1648 – 1658, 2007.

[12] Yuri M. Shtemler, Michael Mond, and Edward Liverts. The Hall instability of unsteady inhomogeneous axially symmetric magnetized plasmas. *Physics of Plasmas*, 11(11):5265–5277, 2004.

[13] V. I. Sotnikov, B. S. Bauer, J. N. Leboeuf, P. Hellinger, P. Trávníček, and V. Fiala. Development of global magnetohydrodynamic instabilities in z-pinch plasmas in the presence of nonideal effects. *Physics of Plasmas*, 11(5):1897–1907, 2004.

[14] J. M. Stone and T. Gardiner. Nonlinear evolution of the magnetohydrodynamic Rayleigh-Taylor instability. *Physics of Fluids*, 19(9):094104, 2007.

DISTRIBUTION:

1 James M. Stone
Department of Astrophysical Sciences,
Princeton University, Princeton, NJ 08544

1 Alexei Poludnenko
LCP & FD, Code 6404, 97/113
Naval Research Laboratory
4555 Overlook Av., S.W.
Washington, D.C. 20375-5344

1	MS 0378	A. C. Robinson, 01431
1	MS 0378	W. J. Rider, 01431
1	MS 0316	J. N. Shadid, 01437
1	MS 1189	C. J. Garasi, 01641
1	MS 1189	T. A. Haill, 01641
1	MS 1189	C. S. Kueny, 01641
1	MS 1189	R. W. Lemke, 01641
1	MS 1189	M. R. Martin, 01641
1	MS 1189	E. P. Yu, 01641
1	MS 1189	H. L. Hanshaw, 01641
1	MS 1189	R. B. Campbell, 01641
1	MS 1106	C. Jennings, 01641
1	MS 0899	Technical Library, 9536 (electronic copy)
1	MS 0359	D. Chavez, LDRD Office, 1911

Sandia National Laboratories